Magnetic and specific heat properties of $YFe_3(BO_3)_4$ and $ErFe_3(BO_3)_4$

2010 J. Phys.: Condens. Matter 22 116006

(http://iopscience.iop.org/0953-8984/22/11/116006)

J. Phys.: Condens. Matter **22** (2010) 116006 (8pp) doi:10.1088/0953-8984/22/11/116006

Magnetic and specific heat properties of $YFe_3(BO_3)_4$ and $ErFe_3(BO_3)_4$

E A Popova[1], A N Vasiliev[2], V L Temerov[3], L N Bezmaternykh[3], N Tristan[4], R Klingeler[4] and B Büchner[4]

[1] Moscow State Institute of Electronics and Mathematics (Technical University), 109028 Moscow, Russia
[2] Low Temperature Physics and Superconductivity Department, Moscow State University, 119991 Moscow, Russia
[3] L V Kirensky Institute of Physics, Siberian Branch of RAS, Krasnoyarsk 660036, Russia
[4] Leibniz-Institute for Solid State and Materials Research IFW Dresden, D-01171 Dresden, Germany

Received 28 October 2009
Published 5 March 2010
Online at stacks.iop.org/JPhysCM/22/116006

Abstract

The present paper reports on the specific heat and magnetization of the $YFe_3(BO_3)_4$ and $ErFe_3(BO_3)_4$ single crystals. In both compounds, antiferromagnetic order of the iron spins evolves at $T_N = 38$ K. The experimental data suggest that the magnetic moments are in the basal plane of the trigonal crystal for both compounds. In the magnetically ordered state the crystal is subdivided into three types of domains, the magnetic moments of the Fe^{3+} ions being aligned along the a axis within each domain. For $ErFe_3(BO_3)_4$, two non-equivalent magnetic positions of the Er^{3+} ions in each domain are observed.

(Some figures in this article are in colour only in the electronic version)

1. Introduction

The family of rare-earth iron borates with the general formula $RFe_3(BO_3)_4$ (R is a rare-earth ion or Y) exhibit a variety of phase transitions and possess a complex magnetic structure which changes as a function of temperature, external magnetic field and substitutions in the rare-earth subsystem. For compounds with R = Y, Eu–Er, a first-order structural phase transition from the $R32$ structure into the less symmetric but also trigonal $P3_121$ one was observed [1, 2]. The temperature of the structural phase transition decreases with increasing ionic radius of the R^{3+} ion. In contrast, the compounds with R = La–Sm do not demonstrate this kind of structural phase transition, i.e. they maintain the $R32$ structure down to the lowest temperatures.

The main motif of the iron borates' crystal structure is spiral chains of edge-sharing FeO_6 octahedra running along the c axis. RO_6 prisms connecting three chains are separated from each other and two kinds of BO_3 triangles are present to connect FeO_6 chains into the three-dimensional structure [3–5].

Every member of the $RFe_3(BO_3)_4$ family exhibits long range antiferromagnetic order at low temperatures. Neutron scattering measurements on Nd, Tb, Ho and Y iron borates show that the magnetic structure is characterized by the propagation vector $\boldsymbol{k} = [0\ 0\ 3/2]$ for both iron and rare-earth ions [6–8]. However, magnetic and spectroscopic measurements [1, 9–11], as well as the fact that the temperature of the antiferromagnetic transition only slightly depends on the particular rare-earth ion, point to the ordering in the iron subsystem only. The rare-earth subsystem remains paramagnetic, being polarized by the staggered magnetic field created by the ordered iron subsystem.

It was found that the magnetic properties of the $RFe_3(BO_3)_4$ single crystals are strongly anisotropic. The orientation of the magnetic moments of both iron and rare-earth ions are governed by the anisotropy of the R^{3+} ion caused by the crystal field. The magnetic moments can change their orientation under the influence of both magnetic field and temperature. In $TbFe_3(BO_3)_4$ [11], the magnetic moments are aligned along the c axis of the crystal in zero magnetic field. The application of magnetic fields parallel to the c axis drives the spin-flop transition in the iron subsystem while the magnetic moments of the Tb^{3+} ions are simultaneously aligned along the external magnetic field [11]. In $GdFe_3(BO_3)_4$ [9, 12, 13], there is a spontaneous spin reorientation at $T = 9$ K from an easy-plane magnetic structure ($T > 9$ K) into an easy-axis configuration

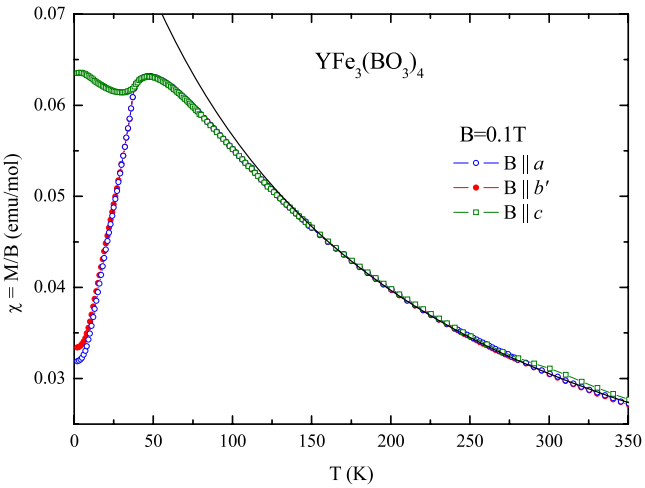

Figure 1. Temperature dependence of the magnetic susceptibility $\chi(T)$ of $YFe_3(BO_3)_4$ measured in the magnetic field $B = 0.1$ T along the a, b' and c axes, respectively (open circles). The solid line corresponds to the Curie–Weiss law.

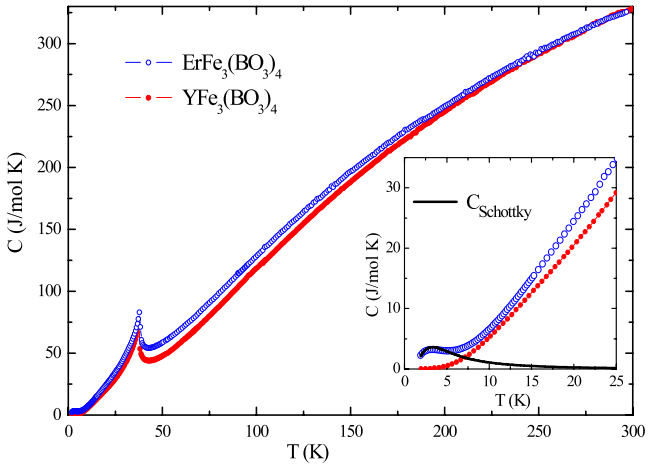

Figure 2. Temperature dependence of the specific heat $C(T)$ of $YFe_3(BO_3)_4$ (closed circles) and of $ErFe_3(BO_3)_4$ (open circles). The inset highlights the temperature range below 50 K. The solid line corresponds to the erbium contribution (Schottky anomaly) in $ErFe_3(BO_3)_4$.

($T < 9$ K). The reorientation of the magnetic moments induced by external magnetic fields is accompanied by a change of the dielectric constant, by a field-induced dielectric polarization and by magnetostrictive effects [14–16]. These effects render $GdFe_3(BO_3)_4$ a linear magnetoelectric since, in external magnetic fields, magnetic, dielectric and possible elastic order evolves. The most pronounced magnetoelectric coupling is observed in $NdFe_3(BO_3)_4$ in which magnetic moments are in the basal plane [17]. So, an identification of the magnetic structure and its response to the external action is the key to understanding the interaction between magnetic, electric and elastic subsystems.

In the present paper we report on the thermodynamic properties of $YFe_3(BO_3)_4$ and $ErFe_3(BO_3)_4$ single crystals. Our experimental data suggest that the magnetic moments are aligned in the basal plane of the trigonal crystal for both compounds. To be specific, the magnetic moments of the Fe^{3+} ions are aligned along one of the a axes of three types of crystal domains. In addition, two non-equivalent magnetic positions of the Er^{3+} ions in each domain are found for $ErFe_3(BO_3)_4$. For both $YFe_3(BO_3)_4$ and $ErFe_3(BO_3)_4$, the complex magnetization processes under an external magnetic field are discussed in detail.

2. Experiment

Single crystals of $YFe_3(BO_3)_4$ and $ErFe_3(BO_3)_4$ were grown using a $Bi_2Mo_3O_{12}$-based flux [18]. The seeds were obtained by spontaneous nucleation from the same flux. The crystals were oriented by means of x-ray diffraction. The magnetic susceptibility $\chi(T)$ was measured in the temperature range 2–350 K in a magnetic field of $B = 0.1$ T using a 'Quantum Design' SQUID magnetometer. The magnetization $M(B)$ was measured at different temperatures in magnetic fields up to 15 T by means of a home-built vibrating sample magnetometer (VSM) [19]. All magnetic measurements were carried out for fields oriented along the crystallographic a, c and b' axes of a trigonal $P3_121$ structure. The latter direction is not a crystallographic axis of the trigonal crystal but points perpendicularly to the crystallographic a and c axes. The heat capacity was measured in the temperature range 2–290 K with a 'Quantum Design' Physical Property Measurement System (PPMS).

3. Results

3.1. $YFe_3(BO_3)_4$

The temperature dependence of the magnetic susceptibility $\chi_a(T)$, $\chi_b(T)$ and $\chi_c(T)$ measured along the a, b' and c axes, respectively, for $YFe_3(BO_3)_4$ are shown in figure 1. At high temperatures, the $\chi(T)$ dependences measured for different orientations of the crystallographic axes with respect to the magnetic field coincide. The magnetic susceptibility follows the Curie–Weiss law with a Weiss temperature $\Theta \approx -133$ K. The negative Weiss constant indicates that the predominant magnetic interactions are antiferromagnetic. The effective magnetic moment amounts to $\mu_{\text{eff}} = 10.3\ \mu_B$, which is in good agreement with the theoretical estimation $\mu_{\text{eff}} = \sqrt{3} g_{\text{Fe}} \sqrt{S(S+1)} \mu_B = 10.2\ \mu_B$ on the assumption of $g_{\text{Fe}} = 2$ and $S = 5/2$ (where g_{Fe} is the g factor and S is the spin of the Fe^{3+} ion). A broad maximum at about 47 K is observed for all field directions. Below 38 K, the magnetic properties become anisotropic. When the applied magnetic field is parallel to the a or b' axes the magnetic susceptibility decreases rapidly upon cooling, while in the case of $B \parallel c$ axis the susceptibility is almost temperature-independent.

The specific heat data in figure 2 exhibit a λ-type anomaly at 38 K. The behavior of both the magnetic susceptibility and the specific heat is typical for antiferromagnetic materials, i.e. our data imply the evolution of long range antiferromagnetic order in $YFe_3(BO_3)_4$ at $T_N = 38$ K. At the lowest measured temperatures, the $\chi_{b'}$ and χ_a exhibit about half of χ_c, which is in contrast to the case of a usual uniaxial

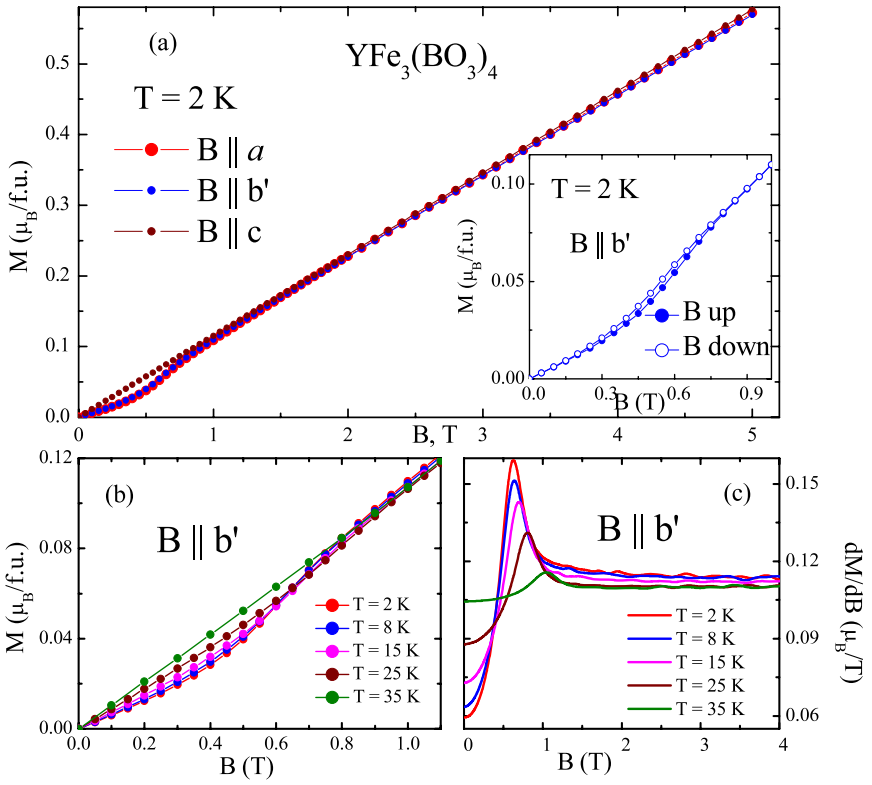

Figure 3. (a) Field dependence of the magnetization $M(B)$ of $YFe_3(BO_3)_4$ measured along the a, b' and c axes, respectively, at 2 K. The inset shows the hysteresis of $M_{b'}(B)$. (b) Field dependence of the magnetization $M_{b'}(B)$ at different temperatures below 1 T. (c) Field dependence of the derivative $dM_{b'}/dB$ at different temperatures.

antiferromagnet where the longitudinal magnetic susceptibility approaches zero at $T = 0$.

The magnetic anisotropy is investigated in more detail by means of magnetization studies at constant temperature, $M(B)$, measured along the a, b' and c axes, as displayed in figure 3(a). While for magnetic fields above ∼1 T the magnetization linearly increases for all field directions, there is a significant anisotropy for smaller fields. The data show a linear M versus B curve for $B \parallel c$ but it is nonlinear for $B \parallel a$ and $B \parallel b'$. In addition, the data imply a slight hysteresis around 1 T as seen in the inset of figure 3(a). The nonlinear behavior of $M(B)$ is a typical feature of a magnetic (spin) re-ordering and the critical field can be derived from the maximum in dM/dB. As can be seen in figures 3(b) and (c), the critical field $B_c \parallel b'$ amounts to ∼0.6 T, at 2 K, and broadens and shifts to slightly higher fields upon heating, i.e. to ∼1 T, at 35 K. Above 1 T, the magnetization curves $M_a(B)$ and $M_{b'}(B)$ are straight lines which can be extrapolated to zero at $B = 0$. The change of the slope of the lines at different temperatures corresponds to a slight temperature dependence of magnetic susceptibility

3.2. $ErFe_3(BO_3)_4$

In contrast to $YFe_3(BO_3)_4$, $ErFe_3(BO_3)_4$ contains two different magnetic ions, i.e. Fe^{3+} and Er^{3+} ions. Its magnetic properties are hence governed by both magnetic subsystems and their interplay. The temperature dependences of the magnetic susceptibility measured along the a, b' and c axes, respectively, for $ErFe_3(BO_3)_4$ are shown in figure 4. The data exhibit a considerable magnetic anisotropy. The $\chi_a(T)$ and $\chi_{b'}(T)$ dependences practically coincide, while χ_c is considerably smaller than χ_a and $\chi_{b'}$ in the whole temperature range under study. Since no significant magnetic anisotropy is expected for the Fe spins, the anisotropy at high temperatures, i.e. far above the magnetic ordering temperature, is attributed to the erbium subsystem. We also mention that, at high temperatures, the data cannot be described in terms of the Curie–Weiss law which again is associated to the Er magnetism. For temperatures larger than the crystal field splitting one would expect the uniform population of the Er levels and, therefore, an isotropic Curie–Weiss-like magnetic susceptibility. The data hence imply that the splitting of the energy levels is at least larger than ∼400 K.

On decreasing the temperature, $\chi_c(T)$ passes through a broad maximum at a temperature of about 70 K and then increases again at low temperature. In contrast, both $\chi_a(T)$ and $\chi_{b'}(T)$ increase monotonically for temperatures as low as 3.4 K where a maximum is observed below which the susceptibility decreases. Note that no difference between the magnetic susceptibility measured in FC and ZFC regimes is observed (inset of figure 4(a)). The evolution of magnetic order is again indicated by a sharp λ-type anomaly at 38 K in the specific heat data (cf figure 2). which implies a second-order magnetic phase transition, as in the case of $YFe_3(BO_3)_4$. Note that a tiny anomaly is also present in $d\chi_c(T)/dT$ at $T_N = 38$ K, as shown in figure 4(a), while $\chi_a(T)$ and $\chi_{b'}(T)$ do not show

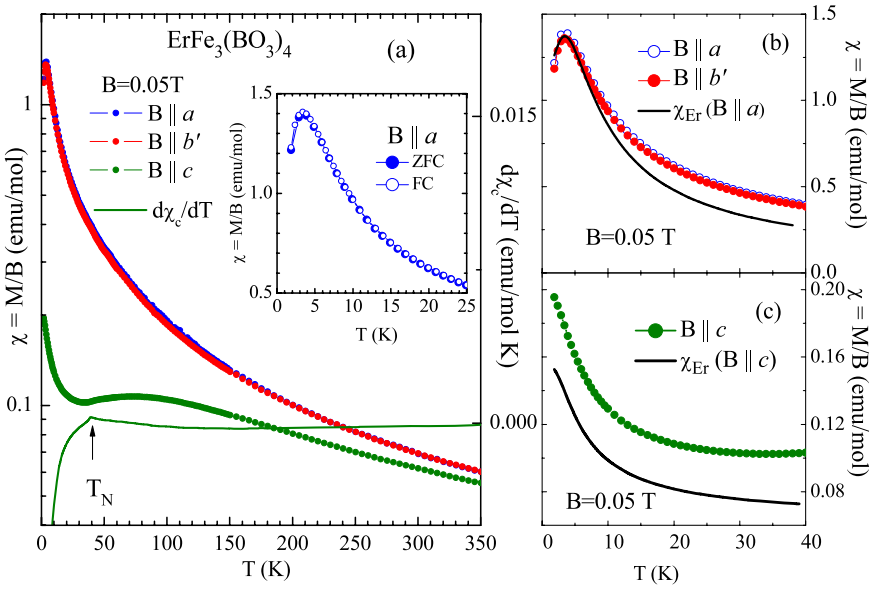

Figure 4. (a) Temperature dependence of the magnetic susceptibility $\chi(T)$ of $ErFe_3(BO_3)_4$ measured in the magnetic field 0.05 T along the a, b' and c axes, respectively (circles). The solid line represents the temperature dependence of $d\chi_c/dT$. The inset shows $\chi_a(T)$ in the FC and ZFC regime. (b) Temperature dependence of the magnetic susceptibility $\chi_a(T)$ and $\chi_{b'}(T)$ below 40 K. The solid line corresponds to the erbium susceptibility below T_N and to the temperature-independent contribution of the iron subsystem (see text). (c) Temperature dependence of the magnetic susceptibility $\chi_c(T)$ below 40 K. The solid line corresponds to the erbium susceptibility below T_N and to the temperature-independent contribution of the iron subsystem (see text).

any signature of the phase transition. We also mention a Schottky-type anomaly in the specific heat data around 3 K, in accordance with the expected splitting of the lowest Er^{3+} Kramers doublet.

The magnetization data $M(B)$ are presented in figure 5. Similar to the temperature-dependent measurements shown in figure 4, the field dependences $M_a(B)$ and $M_{b'}(B)$ also almost coincide in the temperature and magnetic field range under study. As already seen in figure 4, the magnetization measured along the a and b' axes strongly exceeds M_c. Above 5 T, the magnetization $M_c(B)$ obeys a linear behavior while $M_a(B)$ and $M_{b'}(B)$ as well as $M_c(B)$ at $B < 5$ T have a nonlinear character.

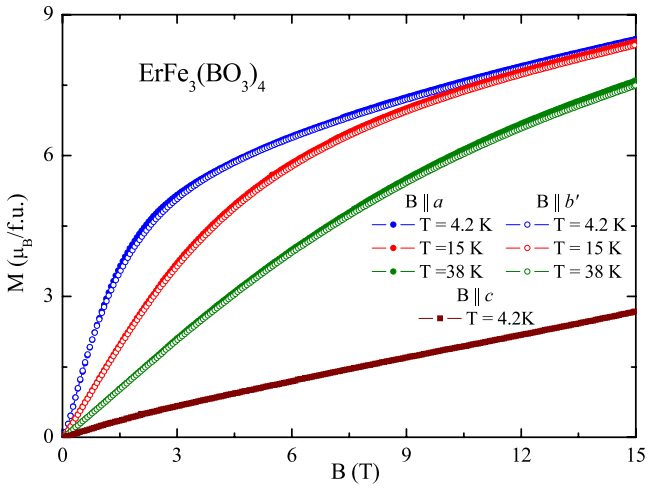

Figure 5. Field dependence of the magnetization $M(B)$ of $ErFe_3(BO_3)_4$ measured along the a, b' and c axes, respectively, at different temperatures.

4. Discussion

4.1. $YFe_3(BO_3)_4$

At $T_N = 38$ K, the onset of long range antiferromagnetic spin order of the iron subsystem in $YFe_3(BO_3)_4$ is demonstrated by both a sharp anomaly in the specific heat and the anisotropic behavior of the magnetic susceptibility measured along and perpendicular to the c axis. The linear dependence of the magnetization $M_c(B)$, the slope of which is almost temperature-independent, as well as the susceptibility data suggest that the magnetic moments of the Fe^{3+} ions are perpendicular to the trigonal c axis of the crystal, i.e. within the (ab') plane.

Below room temperature, both $ErFe_3(BO_3)_4$ and $YFe_3(BO_3)_4$ exhibit a trigonal $P3_12_1$ structure [1, 2]. In this case there are two non-equivalent positions for the iron ions which is in contrast to the $R32$ structure, where all positions of the Fe^{3+} ions are equivalent. The $P3_12_1$ and the $R32$ structure differ from each other by a little shift of one iron chain along the c axis with respect to the other two chains, which from the magnetic point of view is expected to mainly affect the inter- and intra-chain exchange interactions of the iron moments. In the trigonal symmetry, there are three equivalent a axes in the basal plane rotated by $2\pi/3$ along the c axis. In the magnetically ordered state, the crystal is hence subdivided into three types of magnetic domains. In each of them the antiferromagnetic vector **L** characterizing the collinear antiferromagnetic structure is aligned along the

corresponding a axis. Consequently, the value of the total magnetization depends on the orientation of **L** with respect to the external magnetic field in each domain.

The linear part of the measured magnetization curve $M = \chi B$ allows us to estimate the magnetic susceptibility $\chi = \chi_\perp \sin\varphi + \chi_\parallel \cos\varphi$, where φ is the angle between **L** and **B**, $\chi_\perp$ is the transverse magnetic susceptibility measured in the magnetic field $\mathbf{B} \perp \mathbf{L}$ and $\chi_\parallel$ is the longitudinal magnetic susceptibility measured in the magnetic field $\mathbf{B} \parallel \mathbf{L}$.

When the magnetic field is directed parallel to the c axis, the magnetic moments of the Fe^{3+} ions tilt to the c axis, i.e. out of the basal plane. In this case, the antiferromagnetic vector **L** of each domain remains perpendicular to the magnetic field, and the total transverse magnetic susceptibility $\chi_\perp = 0.1154\ \mu_B\ T^{-1}$ is estimated from the slope of the $M_c(B)$ dependence measured at $T = 2$ K.

When the applied magnetic field is perpendicular to the c axis, each domain gives a different contribution to the magnetic susceptibility. If the antiferromagnetic vector **L** of one of the domains is parallel to the magnetic field $\mathbf{B} \parallel a$, the magnetic susceptibility of this domain amounts to $\chi_\parallel$. The other two domains give equal contributions, i.e. $\chi_\parallel + \sqrt{3}\chi_\perp$, so that the total magnetic susceptibility amounts to $\chi_a = \frac{1}{3}(2\chi_\parallel + \sqrt{3}\chi_\perp)$, which is smaller than the one measured along the c axis. Based on the experimental results $\chi_\perp^{Fe} = 0.115\ \mu_B\ T^{-1}$ obtained from the slope of the $M_c(B)$, we estimate $\chi_a = 0.066\ \mu_B\ T^{-1}$ under the assumption that the longitudinal susceptibility is very small at low temperatures. Alternatively, the value $\chi_a = 0.058\ \mu_B\ T^{-1}$ obtained from the slope of the linear part of the magnetization curve $M_a(B)$ below 0.15 T at $T = 2$ K is in good accordance with the experimental data for $\chi_a(T)$ at the lowest measured temperatures, i.e. $\chi_a = 0.057\ \mu_B\ T^{-1}$. The fact that the two estimations of χ_a slightly disagree points to the known small anisotropy of the g factor of the Fe^{3+} ions and a complicated process of magnetization.

The magnetization processes differ from each other for the cases of $B \parallel a$ and $B \parallel b$, respectively. As already pointed out, the antiferromagnetic vector **L** of one of the domains is parallel to the magnetic field when the applied magnetic field is directed along the a axis. The magnetization of this domain is zero as long as the anisotropy is smaller than the Zeeman energy, i.e. below the spin-flop transition where the magnetic moments of this domain flop perpendicular to the external magnetic field. The experimentally observed non-zero magnetization at low fields is mainly caused by the contribution of the other two domains. Here, the antiferromagnetic vectors change their direction upon application of $B \parallel a$ and $B \parallel b$, respectively, until they are perpendicular to the magnetic fields. Note that the antiferromagnetic vector **L** of one of the domains remains perpendicular to the magnetic field in the case of $B \parallel b$, and the spin-flop transition is absent. The similar behavior of $M_a(B)$ and $M_b(B)$ at low fields is possibly caused by the competition of the exchange interaction and anisotropy. For domains with the antiferromagnetic vector **L** deflected from the external magnetic field, **L** skips to the direction perpendicular to the external magnetic field and does not rotate uniformly. The complicated character of the magnetization process is also reflected by the observed hysteresis of the magnetization curve represented in the inset of figure 3(a). Upon heating, the longitudinal susceptibility increases (see figure 4) and the magnetization jump reduces in value and shifts towards higher fields.

In the flop phase **L** is perpendicular to the external magnetic field in the whole crystal. A further increase of the magnetic field leads to a linear increase of the magnetizations $M_a(B)$ and $M_b(B)$ which almost coincides with $M_c(B)$. The tiny difference in the slope of the magnetization curves is probably caused by a small anisotropy of the Fe^{3+} magnetic g factor.

4.2. $ErFe_3(BO_3)_4$

The magnetic properties of $ErFe_3(BO_3)_4$ are governed by both Fe^{3+} and Er^{3+} magnetic subsystems interacting with each other. Usually the strongest magnetic interactions are those within the 3d subsystem, followed by the d–f ones while the f–f interactions are negligible. This latter statement is especially true in the case of the rare-earth iron borates $RFe_3(BO_3)_4$, where the RO_6 prisms in the crystal structure are well isolated from each other, having no common oxygen atoms. Hence these considerations as well as previous studies on rare-earth ferroborates and the similarity to the Y-based material suggest that the magnetic ordering takes place only in the iron subsystem while the erbium subsystem remains essentially paramagnetic, being polarized due to the f–d interaction. We mention that an energy level of the Er^{3+} ion with the total momentum $J = 15/2$ is split into eight Kramers doublets by a crystal field of any symmetry lower than a cubic one. Both the external magnetic field and the staggered magnetic field created by the ordered iron subsystem lead to splitting of the Kramers doublets. The spectroscopic data [20] show that, at zero magnetic field, the splitting between the first and second Kramers doublets amounts to $\Delta = 46\ cm^{-1} = 66.2$ K and the population of the second Kramers doublet is small for $T < T_N$. Hence, below the antiferromagnetic ordering temperature the ground Kramers doublet mainly contributes to the magnetic properties.

As has already been mentioned above, the strong anisotropy of magnetic properties of $ErFe_3(BO_3)_4$ is attributed to the erbium subsystem. In the investigated magnetic field and temperature range, the magnetization measured along the c axis is significantly smaller than the one measured perpendicular to the c axis. This can be caused by smaller values of the out-of-plane g-tensor components of the Er^{3+} ion in comparison to the in-plane ones. Supposedly, the magnetic moments of both the rare-earth and the iron subsystem are not aligned along the c axis of the crystal. As in the case of $YFe_3(BO_3)_4$, the crystal is subdivided into three types of domains. The orientation of magnetic moments within each domain is governed by the local symmetry of the Er^{3+} ion.

In $NdFe_3(BO_3)_4$, the crystal structure of which belongs to the trigonal $R32$ structure, each rare-earth site has three equivalent C_2 axes in the basal plane, and all magnetic positions of the Nd^{3+} ions are equivalent. In contrast, in the

$P3_121$ structure of $ErFe_3(BO_3)_4$ each Er^{3+} site has only one C_2 axis corresponding to the symmetry of strongly deformed triangular prisms ErO_6. There are three non-equivalent magnetic positions of the Er^{3+} ions, the C_2 axes of which are rotated by $2\pi/3$ along the c axis.

In the presence of a magnetic field $\vec{B}$, the Hamiltonian of the Kramers doublet of the Er^{3+} ion with effective spin $S' = 1/2$ in the Cartesian system of coordinates with the z axis along the crystallographic c axis and the x axis along the local C_2 symmetry axis can be written as

$$\hat{H} = \mu_B(B_x g_{xx} S'_x + B_y g_{yy} S'_y + B_y g_{yz} S'_z + B_z g_{zz} S'_z). \quad (1)$$

Here, g_{ij} are the g-tensor components ($i, j = x, y, z$) and B_i, S'_i are the components of the magnetic field and the effective spin, respectively. $B_i = B\cos\varphi_i$, with $\varphi_i = \alpha, \beta, \gamma$, is the angle between the direction of the magnetic field and the local x, y, z axes, respectively. The Hamiltonian gives the energies of the ground Kramers doublet split by magnetic field:

$$E = \pm\tfrac{1}{2}\Delta \quad (2)$$

$$\Delta = \mu_B[(B_x g_{xx})^2 + (B_y g_{yy})^2 + (B_y g_{yz} + B_z g_{zz})^2]^{1/2}. \quad (3)$$

The components of the average magnetic moments are calculated by differentiating equation (2) with respect to the components of the magnetic field:

$$m_x = \mu_B^2 \frac{B_x g_{xx}^2}{2\Delta}\mathrm{th}(\Delta/2kT) \quad (4)$$

$$m_y = \mu_B^2 \frac{B_y(g_{yy}^2 + g_{yz}^2) + B_z g_{yz} g_{zz}}{2\Delta}\mathrm{th}(\Delta/2kT) \quad (5)$$

$$m_z = \mu_B^2 \frac{B_z g_{zz}^2 + B_y g_{yz} g_{zz}}{2\Delta}\mathrm{th}(\Delta/2kT). \quad (6)$$

We emphasize that the components of the magnetic moments refer to local coordinate systems which are placed at the sites of the Er^{3+} ions. Each domain contains one antiferromagnetic vector **L** of the ordered iron subsystem, the direction of which rotates by the angle of $2\pi/3$ along the c axis from one domain to another. The exchange magnetic field B_{ex} directed along the magnetic moment of the Fe^{3+} ion has different effects on the magnetic moments of the Er^{3+} ions at the non-equivalent positions. It causes different Zeeman splittings of the Kramers doublets of the respective Er^{3+} ions.

Depopulation of the upper component of the Er^{3+} ground Kramers doublet split in the magnetic field of the ordered iron subsystem results in a Schottky contribution to the specific heat as is observed in the experiment:

$$C_{Er}(T) = R\left(\frac{\Delta}{kT}\right)^2 \frac{\exp(\Delta/kT)}{(\exp(\Delta/kT)+1)^2}, \quad (7)$$

where R is the gas constant. In the absence of the external magnetic field each domain gives an equal contribution to the specific heat. In general, three non-equivalent magnetic positions within each domain should result in three values of the splitting $\Delta = g_{eff} B_{ex} \mu_B$, where

$$g_{eff} = \sqrt{(g_{xx}\cos\alpha)^2 + (g_{yy}\cos\beta)^2 + (g_{yz}\cos\beta + g_{zz}\cos\gamma)^2}$$

is the effective g factor of the Er^{3+} ions obtained from equation (3). However, the experimental specific heat data are fitted well if we assume that the magnetic state of the erbium subsystem is characterized by only two different values of the ground-state splitting, giving contributions into the total specific heat in the ratio of 1:2. This result suggests that only two non-equivalent magnetic positions of the Er^{3+} ions are present in $ErFe_3(BO_3)_4$. Such a situation can occur if the magnetic exchange field is directed along the a axis of the crystal or at least if it lies in the (ac) plane.

In order to calculate the contributions of the erbium subsystem to the magnetization the influence of both external B and exchange B_{ex} magnetic fields on the magnetic moments of the Er^{3+} ions should be taken in account. The values of both the effective g factor and Kramers doublet splitting calculated by means of equation (3) depend on the value and the direction of the effective magnetic field $\vec{B}_{eff} = \vec{B} + \vec{B}_{ex}$ with respect to local axes of each Er^{3+} ions. This causes the deviation of the Er^{3+} magnetic moments from the direction of the Fe^{3+} magnetic moments within each domain. The contribution of the erbium subsystem to the total magnetization can be calculated as a sum of projections of the magnetic moment components as derived by means of equations (4)–(6) for each Er^{3+} ion of each domain on the direction of the external magnetic field. For the external magnetic field $B \parallel a$, the m_x and m_y components contribute to the total magnetization, while the m_z components should be taken into account in the case of $B \parallel c$.

If we assume that the antiferromagnetically coupled Fe^{3+} moments rotate out of the basal plane (ab'), then the effective field acting on the erbium sublattice with the magnetic moment projections directed opposite to the external field decreases and, therefore, this magnetic moment tends to diminish with increasing field. At the same time, the effective field favors an increase of the magnetization of the erbium sublattice with magnetic moments pointing along the external field. This could lead to a concave character of the magnetization at low fields. However, the experimental data do not show such behavior. Upon increasing the external magnetic field the antiferromagnetic vector **L** of the ordered iron subsystem tilts and the spin-flop transition occurs at a critical field. Usually, the spin-flop is associated with a jump of the magnetization. The experimental data, however, do not show such a jump, which might imply that the magnetic moments of the Fe^{3+} ions are aligned along the a axis and do not rotate out of the (ab') plane.

The contribution of the erbium subsystem to the specific heat $C(T)$ and the magnetic susceptibility $\chi_a(T)$ and $\chi_c(T)$ is shown by the solid lines in figures 2 and 4, respectively. The fitted parameters $g_{xx} = 8.7$, $g_{yy} = 10.5$, $g_{zz} = 2$, $g_{yz} = 2.5$ and $B_{ex} = 1.2$ T (at $T = 2$ K) provide the best agreement with the experimental data. We mention that the decrease of B_{ex} upon increasing the temperature up to T_N has been taken into account for the fitting. We also note that the contribution of the ordered iron subsystem was taken as a constant equal to the value at 2 K when calculating $\chi(T)$. As is visible in figure 4, upon increasing the temperature up to T_N the calculated data $\chi(T)$ deviate from the experimental results.

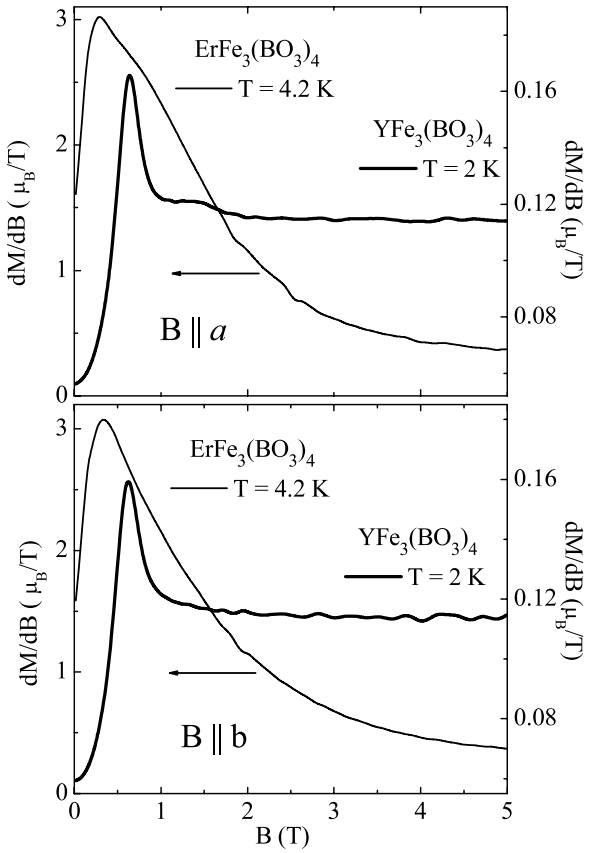

Figure 6. Field dependence of the derivative $dM_{b'}/dB$ at lowest measured temperatures for $YFe_3(BO_3)_4$ and $ErFe_3(BO_3)_4$.

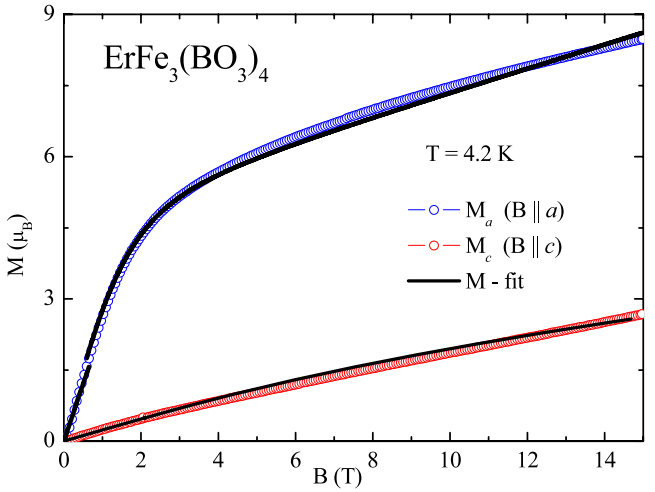

Figure 7. Field dependence of the magnetization $M(B)$ of $ErFe_3(BO_3)_4$ measured along the a and c axes, respectively, at 4.2 K. The solid line corresponds to the calculated total magnetization of the iron and the erbium subsystem (see text).

We attribute this deviation to the temperature dependence of the iron subsystem, which should have a similar character as in the case of $YFe_3(BO_3)_4$, under the assumption that magnetic moments of the Fe^{3+} ions in $ErFe_3(BO_3)_4$ are aligned along the a axis.

The calculated total magnetization of the iron and the erbium subsystem, i.e. $M_c = M_c^{Fe} + M_c^{Er}$, is shown by the solid line in figure 7. For $B \parallel c$ the magnetic moments of the Fe^{3+} ions tilt in the direction of the external magnetic field, giving rise to a linear magnetic field dependence $M_c^{Fe} = \chi_\perp^{Fe} B$. The linear part of the magnetization curve $M_c(B)$ allows us to estimate the transverse susceptibility of the iron subsystem: $\chi_\perp^{Fe} = 0.113\ \mu_B\ T^{-1}$. All domains contribute equally, while the Er^{3+} ions within each domain give different contributions because of magnetically non-equivalent positions.

The comparison of the experimental data dM/dB versus B, for $YFe_3(BO_3)_4$ and $ErFe_3(BO_3)_4$, represented in figure 6 suggests that the magnetization process is similar for both compounds. The spin-flop transition in the iron subsystem occurs in the domain with the antiferromagnetic vector **L** parallel to the a axis. The antiferromagnetic vectors of the other domains tilt perpendicular to the magnetic field. In the flop phase, **L** is uniform in the whole crystal and is perpendicular to the external magnetic field. Note the spin-flop transition takes place in the magnetically ordered iron subsystem and the magnetic moments of the erbium subsystem follow the iron spins. The responses of magnetically non-equivalent Er^{3+} ions of each domain to the external magnetic field are different. The deviation of the calculated dependence $M(B)$ from the experimental data indicates an anisotropy of the f–d exchange interaction which is expected due to strong spin–orbital interaction in the Er^{3+} ions. To be specific, if the magnetic moments of the Fe^{3+} ions tilt under the influence of the magnetic field the angle between the Fe^{3+} and Er^{3+} magnetic moments can change, thereby causing the angular dependence of the f–d interaction.

An essential structural feature of $YFe_3(BO_3)_4$ and $ErFe_3(BO_3)_4$ is the presence of iron chains. The broad maximum at 40 K in $\chi_c(T)$ for $YFe_3(BO_3)_4$ and at 70 K in $\chi_c(T)$ for $ErFe_3(BO_3)_4$ is possibly caused by the low dimensionality of the iron magnetic system [21]. In [22], the following formula has been proposed to model the magnetic susceptibility of the Heisenberg antiferromagnetic spin chain with $S = 5/2$:

$$\chi_{Cr} = \frac{N_A S(S+1) g^2 \mu_B^2}{3kT} \frac{1+u(K)}{1-u(K)}, \qquad (8)$$

where

$$u(K) = \coth K - \frac{1}{K}, \qquad K = -\frac{2JS(S+1)}{kT}.$$

Here, the intra-chain exchange parameter J is positive for antiferromagnetic coupling inside the chain, i.e. $H_{exch} = 2J \sum_{i>j} \mathbf{S}_i \mathbf{S}_j$. This function has already been successfully applied for various spin chain compounds [23–26]. The position of the broad maximum observed in the experimental $\chi(T)$ data indicates $J = 5.7$ K for $YFe_3(BO_3)_4$ and $J = 8.6$ K for $ErFe_3(BO_3)_4$. We note that a noticeable deviation of the magnetic susceptibility from the Curie–Weiss law below $\sim$150 K $\gg T_N$ suggests that short range spin correlations remain at temperatures well above T_N, which is a characteristic feature of low-dimensional systems.

5. Conclusions

The temperature dependence of the specific heat and the magnetic susceptibility as well as the field dependence of the magnetization of $YFe_3(BO_3)_4$ and $ErFe_3(BO_3)_4$ single crystals is presented. For both compounds, antiferromagnetic ordering evolves at $T_N = 38$ K. In $ErFe_3(BO_3)_4$, the rare-earth subsystem remains paramagnetic down to 2 K, being polarized by the staggered magnetic field created by the ordered iron subsystem. The splitting of the ground Kramers doublet by the transferred staggered field results in Schottky contributions to the specific heat and the magnetic susceptibility as observed in the experiment. The analysis of the experimental data suggests that the magnetic moments are in the basal plane of the trigonal crystal for both compounds. The crystal is subdivided into three types of domains, and the magnetic moments of the Fe^{3+} ions are aligned along one of the *a* axes of the crystal within each domain. Two non-equivalent magnetic positions of the Er^{3+} ions in each domain of $ErFe_3(BO_3)_4$ were observed. Anisotropy of the Er^{3+} ion leads to a deviation of magnetic moments from the direction of the exchange magnetic field created by the ordered iron subsystem. The magnetic structure of $YFe_3(BO_3)_4$ and $ErFe_3(BO_3)_4$ results in a complicated magnetization processes under external magnetic field. In the magnetic field parallel to the *a* axis, the flop phase is realized at $B > 1$ T, i.e. the magnetic moments of the Fe^{3+} ions are perpendicular to the external magnetic field.

Acknowledgments

This work was supported by DFG grants 436 RUS and HE 3439/6 (FOR 520). The authors are indebted to M N Popova and B Z Malkin for valuable discussions.

References

[1] Hinatsu Y, Doi Y, Ito K, Wakeshima M and Alemi A 2003 *J. Solid State Chem.* **172** 438
[2] Fausti D, Nugroho A A, van Loosdrecht P H M, Klimin S A, Popova M N and Bezmaternykh L N 2006 *Phys. Rev.* B **74** 024403
[3] Joubert J-C, White W B and Roy R 1968 *J. Appl. Crystallogr.* **1** 318
[4] Campá J A *et al* 1997 *Chem. Mater.* **9** 237
[5] Klimin S A, Fausti D, Meetsma A, Bezmaternykh L N, van Loosdrecht P H M and Palstra T T M 2005 *Acta Crystallogr.* B **61** 481
[6] Fischer P, Pomjakushin V, Sheptyakov D, Keller L, Janoschek M, Roessli B, Schefer J, Petrakovskii G, Bezmaternikh L, Temerov V and Velikanov D 2006 *J. Phys.: Condens. Matter* **18** 7975
[7] Ritter C, Balaev A, Vorotynov A, Petrakovskii G, Velikanov D, Temerov V and Gudim I 2007 *J. Phys.: Condens. Matter* **19** 196227
[8] Ritter C, Vorotynov A, Pankrats A, Petrakovskii G, Temerov V, Gudim I and Szymczak R 2008 *J. Phys.: Condens. Matter* **20** 365209
[9] Levitin R Z, Popova E A, Chtsherbov R M, Vasiliev A N, Popova M N, Chukalina E P, Klimin S A, van Loosdrecht P H M, Fausti D and Bezmaternykh L N 2004 *JETP Lett.* **79** 531
[10] Chukalina E P, Kuritsin D Yu, Popova M N, Bezmaternykh L N, Kharlamova S A and Temerov V L 2003 *Phys. Lett.* A **322** 239
[11] Popova E A, Volkov D V, Vasiliev A N, Demidov A A, Kolmakova N P, Gudim I A, Bezmaternykh L N, Tristan N, Skourski Yu, Büchner B, Hess C and Klingeler R 2007 *Phys. Rev.* B **75** 224413
[12] Balaev A D, Bezmaternykh L N, Gudim I A, Temerov V L, Ovchinnikov S G and Kharlamova S A 2003 *J. Magn. Magn. Mater.* **258/259** 532
[13] Pankrats A I, Petrakovskii G A, Bezmaternykh L N and Bayukov O A 2004 *JETP Lett.* **99** 766
[14] Yen F, Lorenz B, Sun Y Y, Chu C W, Bezmaternykh L N and Vasiliev A N 2006 *Phys. Rev.* B **73** 054435
[15] Zvezdin A K, Kadomtseva A M, Krotov S S, Pyatakov A P, Popov Yu F and Vorob'ev G P 2006 *J. Magn. Magn. Mater.* **300** 224
[16] Zvezdin A K, Krotov S S, Kadomtseva A M, Vorob'ev G P, Popov Yu F, Pyatakov A P, Bezmaternykh L N and Popova E A 2005 *JETP Lett.* **81** 272
[17] Zvezdin A K, Vorob'ev G P, Kadomtseva A M, Popov Yu F, Pyatakov A P, Bezmaternykh L N, Kuvardin A V and Popova E A 2006 *JETP Lett.* **83** 509
[18] Bezmaternykh L N, Temerov V L, Gudim I A and Stolbovaya N L 2005 *J. Crystallogr. Rep.* **50** (Suppl 1) 97
[19] Klingeler R, Büchner B, Choi K-Y, Kataev V, Ammerahl U, Revcolevschi A and Schnack J 2006 *Phys. Rev.* B **73** 014426
[20] Popova M N and Chukalina E P, private communication
[21] de Jongh L J and Miedema A R 2001 *Adv. Phys.* **50** 947
[22] Wagner G R and Friedberg S A 1964 *Phys. Lett.* **9** 11
[23] Grey I E and Steinfink H 1971 *Inorg. Chem.* **10** 691
[24] Nakayama N, Kosuge K, Kachi S, Shinjo T and Takada T 1980 *J. Solid State Chem.* **33** 351
[25] Dingle R, Lines M E and Holt S L 1969 *Phys. Rev.* **187** 643
[26] Barnes A D J, Baikie T, Hardy V, Lepetit M-B, Maignan A, Young N A and Grazia Francesconi M 2006 *J. Mater. Chem.* **16** 3489